metals

MDPI

Article

Hot Deformation Behavior of C-Mn Steel with Incomplete Recrystallization during Roughing Phase with and without Nb Addition

Grega Klančnik [1,*], Jan Foder [2], Boštjan Bradaškja [2], Mina Kralj [2], Urška Klančnik [3], Paul Lalley [4] and Douglas Stalheim [5]

[1] Pro Labor d.o.o., Podvin 20, 3310 Žalec, Slovenia
[2] SIJ Acroni d.o.o., Cesta Borisa Kidriča 44, 4270 Jesenice, Slovenia
[3] Valji d.o.o., Železarska Cesta 3, 3220 Štore, Slovenia
[4] CBMM Europe, Zuidplein 96, 1077 XV Amsterdam, The Netherlands
[5] DGS Metallurgical Solutions, Inc., 15003 NE 10th Street, Vancouver, WA 98684, USA
* Correspondence: grega.klancnik@prolabor.si

Abstract: The objective of the study is to improve understanding of the practical role of niobium (Nb) in the case of industrial inconsistent rolling processes such as the rolling of heavy gauge plates where a lower stored energy rolling practice will result in a less stable and less repeatable static recrystallization (SRX) activation that prevents complete recrystallization. In the current study, these variabilities are validated by comparing the mean flow stress (MFS) indirectly determined from the rolling force measured on a reverse four-high rolling mill stand. The material resistance to deformation and grain size evolution of a C-Mn steel during hot rolling was observed and validated with and without Nb addition. The pre-defined rolling schedule was predicted to exhibit incomplete recrystallization in the roughing phase due to the limited stored energy of deformation that resulted from low rolling loads and a higher number of rolling passes. The prior austenite grain size (PAGS) distribution was predicted and compared to the measured effective ferrite grain (FG) size distribution after the completion of hot rolling and phase transformation achieved using natural air plate cooling. Both the predicted PAG and measured FG distributions revealed the presence of multimodality, and both distributions were used for grain size reduction factor determination for $\gamma \rightarrow \alpha$ transformation for the current study with 1.96 for 0 Nb and 1.70 for 240 Nb. The results presented in this paper are not only limited to the rolling schedule used in this paper because instabilities resulting in incomplete austenite conditioning are also observed when evaluating the cross-sections of other heavy plates and various steel grades utilizing different processing routes with comparable compositions such as modern lean abrasion-resistant steels, regular line pipe steels, and other similar grades.

Keywords: C-Mn steel; hot rolling; niobium; recrystallization; heavy plates; CALPHAD

check for updates

Citation: Klančnik, G.; Foder, J.; Bradaškja, B.; Kralj, M.; Klančnik, U.; Lalley, P.; Stalheim, D. Hot Deformation Behavior of C-Mn Steel with Incomplete Recrystallization during Roughing Phase with and without Nb Addition. *Metals* **2022**, *12*, 1597. https://doi.org/10.3390/met12101597

Academic Editors: Hailiang Yu, Liqing Chen, Haitao Gao and Yun Zhang

Received: 23 August 2022
Accepted: 16 September 2022
Published: 25 September 2022

Publisher's Note: MDPI stays neutral with regard to jurisdictional claims in published maps and institutional affiliations.

Copyright: © 2022 by the authors. Licensee MDPI, Basel, Switzerland. This article is an open access article distributed under the terms and conditions of the Creative Commons Attribution (CC BY) license (https://creativecommons.org/licenses/by/4.0/).

1. Introduction

The effect of strain (deformation)-induced precipitation (SIP, DIP) in Nb microalloyed steels is well documented and understood [1]. Carbonitride, carbide, or nitride precipitates (MXs, where M is the microalloying metal and X is the interstitial element) retard the recrystallization by pinning the dislocations and austenite grain and subgrain boundaries [2]. In this paper, Nb as a microalloying element is emphasized. An important aspect, when it comes to recrystallization, is Nb in solid solution, which also retards the recrystallization by solute drag effect [3]. Useful tools for predicting whether the Nb is in austenite solution or in form of precipitates are solubility products calculated for Nb, C, and N in austenite. There have been numerous equations posted by different researchers in the past [4,5]. In addition, the Calculation of Phase Diagrams (CALPHAD) approach can be used for multicomponent systems for equilibrium and homogeneous precipitation of non-deformed

austenite for estimation of free [Nb] in austenite before the roughing phase is conducted, for example by using commercial software such as Thermo-Calc (Thermo-Calc 2022a software AB, TCFE 11.0, Stockholm, Sweden) [6].

1.1. Roughing Stage

In the case of plate rolling, the specific recrystallization stop temperature (RST) and recrystallization low temperature (RLT) are commonly replaced due to practicality by semi-empirical equations for non-recrystallization temperature, *T*nr, using the most common equations found in [7]. Thereby, the instabilities and influence on mechanical properties can be studied by successive deformations in the temperature regions close to RLT and RST. This is not so straightforward when considering industrial conditions. However, the material can be processed using a certain reduction percentage close to this unstable region towards completion of the roughing phase and compared to other rolling schedules. It is recognized that heterogeneous microstructures with regions of large grains give poor toughness and that these areas can form in the temperature regions where recrystallization is sluggish; therefore, rolling is commonly performed far above and under RST [1]. In the current study, the reductions for roughing were carried out using limited rolling loads. Both roughing and finishing are strictly separated as typical industrial two-step control rolling with reductions completed sufficiently above and under *T*nr. Based on actual effective strain (ε) performed during the roughing phase, the main post-deformation softening mechanism is recognized to be static recovery (SRV) and static recrystallization (SRX) when deformation is above the critical stress—the deformation needed for static recrystallization start ($\sigma_{cs}, \varepsilon_{cs}$)—but also far below the critical deformation start (ε_{cD}) for dynamic and metadynamic recrystallization to initiate (DRX, MDRX) [8]. The latter is more probable for thin plate, wire, or sheet rolling where lower temperatures with sufficient cumulative strain are common [9–11]. Additionally, based on [5], the needed strain for dynamic recrystallization (DRX) should be above 14% reduction in thickness, and in our case, the whole roughing stage was conducted using a close-to-linear trend beginning from 9 to 15% of reduction (R1, 8.63–8.76%; R2, 11.53–11.78; R3, 13.16–13.22%; R4, 15.02–15.15%; R5, 15.03–15.12%; R6, 14.98–15.07%, R7, 15.05–15.09%). Based on Gleeble hot-compression tests, the minimum for the chemical composition in this study for DRX should be above 12.2–16.49% for 1 s^{-1} and 3 s^{-1} determined at rouging temperature 1150 °C with $\varepsilon = 0.8$ to observe DRX phenomena. As discussed, the grain refinement produced under recrystallization rolling (RR) is highly dependent on the chosen rolling schedule [12].

1.2. Finishing Stage

Deformation, when MXs are considered, greatly accelerates carbonitride precipitation kinetics due to the higher number of nucleation sites (N_0) and involved diffusivity of Nb (D) at a given temperature in austenite. Importantly, the effects of deformation on precipitation kinetics are observed through the effects on flow stress [13]. Potential nucleation sites for carbonitride precipitation are dislocation nodes in a three-dimensional network of dislocations and the subgrain boundaries; thus, increasing dislocation density increases the number of carbonitride nucleation sites [14,15]. Based on [15], potential nucleation sites per volume (in m^{-3}) for an MX are estimated as:

$$N_0 = 0.5 \times \rho^{1.5} \tag{1}$$

by knowing the dislocation density (in m^{-2}), which is estimated from the flow and yield stress (as dependent on grain size, particles, and solute atoms) for particular deformation temperature of interest, knowing the Taylor factor, material constant, shear modulus, and Burgers vector, ρ, $\sigma, \sigma_y, T, M, \alpha, \mu/G$, and b, as proposed by [15].

In addition, deformation causes excess vacancies, which can be attracted to Nb atoms to form Nb–vacancy complexes. Such complexes cause non-equilibrium Nb segregation to vacancy sinks, such as dislocation cell walls and grain boundaries, which leads to enhancement of precipitation [16].

In addition, besides retarded recrystallization, strain-induced carbonitride precipitation strengthens austenite by precipitation strengthening and has an influence on the extent of potentially retained work (or strain hardening) and achieved grain refinement influencing the final mechanical properties [17].

Material resistance during hot rolling can be measured by an indirect method using calculated mean flow stress (MFS) from measured vertical rolling force (FR) as shown in the previous study [18] based on the simplified Sims model [19] and used in numbers of papers [20,21]. Observation of MFS elucidates the material softening and strain hardening phenomena in processed C-Mn steel based on rolling schedules and chemical compositions. It is understood that non-uniform cross-sectional microstructure produced by hot rolling (or forging) causes scatter in final mechanical properties due to limited, less uniform cross-section dislocation density affecting related N_0 for MX precipitation, influencing the cross-section effective PAG refinement and the uniformity of the final transformed microstructure [22,23]. In the current study, these instabilities are tested with and without introduced Nb.

2. Experimental Section

In the current study, a C-Mn steel was studied during and after the industrial hot-rolling process. Predictions were made based on different reheat temperatures using the hot rolling simulation model MicroSim. The interpass times used in the simulation were adjusted for the middle length of a plate for each per-pass reduction. Additionally, restricted successive per-pass reductions in the roughing stage (R1 to R7) and limited interpass times (controlled by rolling speed) were tested. Partial per-pass SRX of austenite was recognized under such rolling conditions in the roughing stage as a starting condition for entering the final rolling stage performed after time delay for both compositions with and without Nb (F1 to F4). The calculated low reheat slab temperature was achieved using cold-charged/indirect technology. The chosen temperature was sufficient for having all the Nb in solid solution in austenite before the roughing phase began, according to Thermo-Calc. This is important for effective and homogeneous precipitation of Nb(C,N) during rolling. For both compositions (Table 1), similar target reheating times and temperatures were used, also affecting the achieved finish rolling temperature (FRT) with a close to constant time delay. A two-stage rolling was adapted here with the final passes conducted in predetermined temperature intervals for achieving the needed final material characteristics comparable to the off-line normalized state. Therefore, the additional step of off-line heat treatment in this experimental study was not necessary and is not included in the study. Calculated MFS values were compared for both compositions. The starting slabs (200 mm × 2030 mm) were reheated between 1180 and 1200 °C for Nb-added steel (240 Nb) and base composition (0 Nb). The absolute temperature deviation was +/− 10 °C. No broad sizing was performed. The majority deformation was taken in the main rolling direction, and the first R1 was taken as the actual roughing per-pass reduction (in %). For both plates, comparable final cooling rates are achieved by natural cooling under air due to the same plate geometry and use of sequential rolling. The susceptibility for bainite transformation, especially for the 240 Nb sample, is estimated to be low due to the limited internal slab segregation severity, chemical composition, and achieved slow plate cooling.

Table 1. Chemical composition of the studied C-Mn steel plates (in mass %).

Sample	Nb *	C	Si	Mn	P	S	Cr	Cu + Ni	Mo	N *	CEV
0 Nb	0	0.16	0.44	1.24	0.017	0.0005	0.22	0.54	0.05	78	0.46
240 Nb	240	0.16	0.42	1.22	0.016	0.0002	0.22	0.59	0.04	68	0.45

* in ppm.

The C-Mn steel plates were rolled into the final thickness of 45 mm from a slab thickness of 200 mm. In the case of both compositions, a total reduction of 65% was performed in the roughing stage (R), and reduction was made in the finishing phase (F) with 35% of deformation (after time delay) for triggering the strain-induced Nb(C,N) precipitation in the case of 240 Nb.

Samples were extracted from the same sample positions for gathering sufficient data for statistical evaluation of obtained mechanical properties, observing the changes and role of Nb addition under variable production conditions with an emphasis on the measured scatter of mechanical properties for the rolling schedule. For this study, a rather reasonably high total metallurgical reduction ratio was used; slab:plate = 4.4:1. The austenite conditioning is expected to be restricted by decreasing the metallurgical ratio for the same percentage of per-pass reduction, also resulting in thicker plate exit height, h.

For the kinetic study of PAG evolution during simulated rolling schedule (SRS), the tool MicroSim was used [22] as discussed already. MicroSim is a physical model based on extensive research for predicting the flow stress responses and therefore temperature adjustments between measured and predicted MFS. The latter is used for best-fit validation of on-line material deformation response. A quantification of the softening processes occurring during multistage deformations on flow stress is described also in [8] using other predictive and unified constitutive models. Due to rather light per-pass reductions used in the presented experimental work, an FEM numerical model was also used (finite element method, Abaqus 6.13, Dassault Systèmes, Simulia Corp., Providence, RI, USA) to simulate the penetration efficiency and uniformity of stress/deformation from the surface toward the center of a plate for each roughing pass. For FEM simulation a complete SRX was considered; a common to full recrystallization-controlled rolling (RCR) or recrystallization rough rolling (RRR) process was used to identify the minimum penetration depth as a boundary condition of the proposed rolling schedule. FEM methods are well-accepted methods for optimization of deformable materials [24] and were therefore used also in this study.

Like in our previous study on ultrahigh-strength steel (UHSS) [18], the hot deformation behavior of C-Mn steel was also studied during successive reductions and evaluated by MFS as presented further in the paper. The focus is given not only on the roughing stage but also on the finish rolling stage where strain-induced precipitation is expected (for 240 Nb) in partly recrystallized austenite [18].

For microstructure investigation, the samples were prepared following standard metallographic procedures of grinding (SiC polishing paper: 120, 220, 320, 500, and 1200 grit size) and polishing (with 0.05 µm alumina emulsion) and etching using Nital (4 vol.% solutions of nitric acid in ethanol). The microstructure was investigated using light optical microscopy (LOM) (Zeiss, Zeiss Axio Imager M2m, Francoforte, Germany) and a high-resolution scanning electron microscope (FE-SEM) (Zeiss Supra VP55, Francoforte, Germany and using INCA). A scanning transmission electron microscopy (STEM) (Zeiss Supra VP55, Francoforte, Germany) detector was also used on the thin TEM samples using extraction carbon replicas and a Cu-based grid holder for confirming the presence of nano-sized Nb(C,N) in the as-deformed state in the 240 Nb sample (bright field imaging). The reader can find more details about the sampling in [25]. Basic mechanical properties such as strength ($R_{p0.2}$, R_m) and elongation (A_5) were measured using a Zwick/Roell Z600 according to EN ISO 6892-1:2017 B60, and average transverse low-temperature toughness was measured using V-notch (at −20 °C for quality J2 based on EN 10025-2) by using three impact test pieces according to EN ISO 148-1:2016 [26,27]. The samples were extracted based on the procedure described in EN 10025-2 [28].

For quantitative pearlite determination and estimation of potential changes in the R_m, the equation by Pickering was taken from [29]. The FG size distribution was determined using ImageJ software (ImageJ 1.53k, open source software, NIH, Bethesda, MD, USA) by manually outlining the FG crystal boundaries on FE-SEM micro-photographs and the results are presented by Feret's diameter. ImageJ and the method itself are well accepted for

micro-scale grain size analysis of the achieved final microstructural state. The reconstruction of PAG can also be implemented (not necessary in this case) instead of simply observing FG, by using electron backscatter diffraction (EBSD) [30,31]; however, due to the sufficient repeatability of the presented method and the possibility of large metallographic section investigation and direct correlation with mechanical properties, the work was performed by analyzing the final FG size distribution only. The reconstruction of PAG from a known FG size is still possible for similar rolling schedules and cooling rates and compositions if the grain size reduction factor of $\gamma \rightarrow \alpha$ transformation is known, as described in Section 3.7.2.

Prediction of equilibrium Nb solubility temperature and other equilibrium solvus temperatures as well as the equilibrium volume fraction of Nb(C,N) at temperatures of interest was performed under the presumption that equilibrium Nb content in austenite is reached. The calculation was performed using Thermo-Calc software (Thermo-Calc 2022a, Thermo-Calc Software AB, Stockholm, Sweden) with the correspondent TCFE11.0 database.

Reconstruction of the CCT diagrams was completed using an internal experimental database and by using the KIN program (SMS group).

Additionally, the thermo-mechanical simulator GLEEBLE 1500D (Gleeble, Gleeble 1500, Digital control, Poestenkill, NY, USA) was also used for the determination of critical deformations, ε_{cD}, and for PAG growth studied during the temperature–time delay between the roughing and finishing phase. It should be remembered that the values of ε_{cD} and t_{50} are also dependent on grain size, D_0, and sensitive to the industrial rolling schedule. For determination of the lower limit for PAGS refining in the roughing stage, hot-compression tests were performed by activating DRX, and the samples were water quenched after hot compression at elevated temperature to prevent any PAG growth.

The general composition, presented in Table 1, was determined by optical emission spectroscopy, ARL MA-310. Carbon and sulfur were determined as in [18] by combustion method using LECO CS-600 (CS 600 series, LECO Corporation, St. Joseph, Michigan, MI, USA) and nitrogen by LECO TC-500 (TC 500, RO 500, TN 500 series, LECO Corporation,St. Joseph, Michigan, MI, USA).

3. Results and Discussion

3.1. Materials

The chemical composition presented in Table 1 reveals that studied C-Mn steel has a low carbon content and a limited equivalent CEV for weldability based on the IIW equation. The banding tendency is taken as comparable for both compositions (Mn, P, Si) and therefore has a similar influence on the A_{r3} [32] as well as on the A_{e3}, shown later. Produced heats are aluminum killed (>0.02%, Al:N $\geq$ 2:1), vacuum degassed, and cast into slabs using a short-bow continuous caster (CC).

Based on Table 1, the solid-solution hardening is considered comparable between heats. As Mn and C have an influence on the pearlite content (and bainite transformation) potentially affecting tensile stress, both elements are restricted for samples 0 Nb and 240 Nb. The relatively high Nb content in 240 Nb allows a sufficient phase fraction of Nb(C,N) needed for the Zener pressure for MFS comparison. An equation for ferrite–pearlite steels provided by Pickering was taken from [5,29,32] and used for strength estimation. Similar compositions are found for flat structural products as they are common for so-called commodity grades as presented in [33]; if needed, they are modified by introducing V for controlled post-rolling precipitation for additional strength increase. For V and Nb microalloyed grades, natural cooling is not considered an optimal process for repeatable cooling paths achieved on the plate.

3.2. Rolling Procedure

MicroSim was used for the evaluation of the SRX fraction under different SRS levels. An example is shown for the 240 Nb sample in Figure 1. By increasing the slab temperature, even for the schedule with low stored energy deformation (low engineering reduction,

e, and low true deformation per pass, ε), recrystallization kinetics is enhanced, despite PAG coarsening. This is interpreted as the result of lower Zener pressure (predominately in finishing) and lowered solute drag (in roughing) due to enhanced grain and subgrain boundary mobility at higher temperatures. A fluctuation of recrystallization phenomena under weak roughing passes (with low rolling forces) is observed regardless of the chosen temperature. The SRX becomes gradually more stable from pass to pass as presented in Figure 1 for the highest temperature only. It should be remembered that the degree of SRX fluctuation and retained strain after a certain holding (interpass) time is also affected due to dislocation mobility (*M*) and is specific for composition and temperature. This is usually obtained by fitting the experimental data [12]. On contrary, by decreasing the slab temperature, as shown in Figure 1, the softening resulting from SRX becomes less pronounced, especially in the region close to homogeneous secondary precipitation of Nb(C,N). Based on [1,5,34] and the data presented in this paper, the importance of proper slab reheating temperature adjustment is revealed, as it not only influences the starting PAGS and achieved solubility of carbo-nitrides, but also affects the roughing temperature profile and with that the temperature positioning of the last roughing pass (to prevent entering into the area between RLT and RST and achieving final FRT when close to constant time delay is used. Based on [12], real deformation per pass needed for activating SRX is above $\varepsilon = 0.06$ (5.9% of engineering reduction), and the progress of SRX kinetics is controlled with the holding time and optimized in relation to t_{50}. In the case of Nb addition, a more sluggish SRX is expected, and therefore a longer t_{50} for roughing and finishing stage is expected (Figure 2).

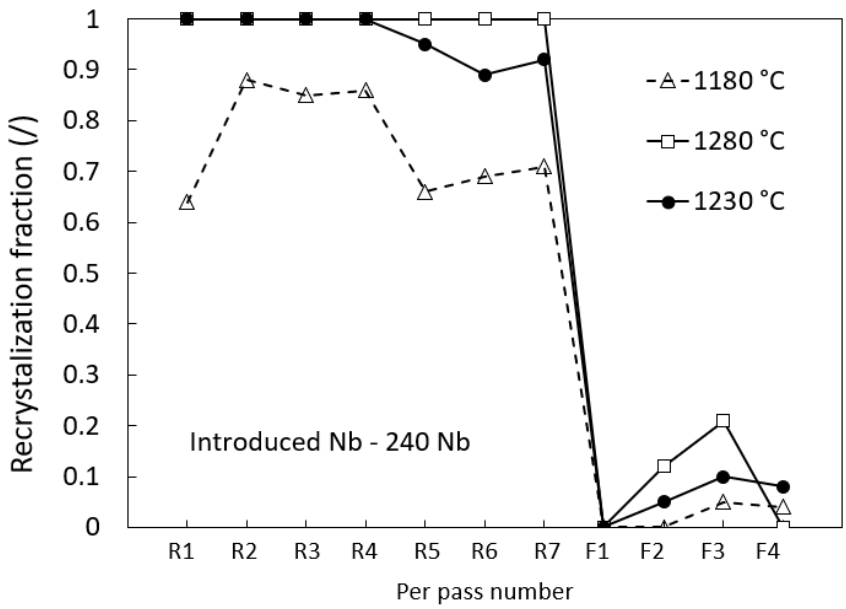

Figure 1. SRS prediction: Influence of predicted slab reheating temperature and SRX development as a measure for velocity of grain boundary movement during the equal interpass in the case of sample 240 Nb between 1180 and 1280 °C. The temperature drops, present during industrial rolling from the furnace to R1, were also considered.

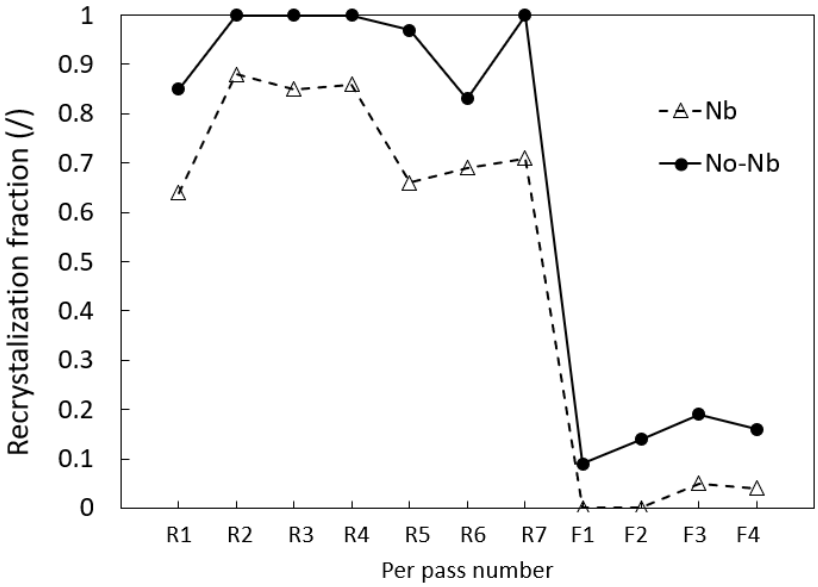

Figure 2. Recrystallization fraction of both compositions (0 Nb, 240 Nb) based on low-temperature slab reheating regime. Both compositions are predicted with incomplete recrystallization in the roughing stage whereas the lowest SRX is achieved with 240 Nb.

At lower reheating temperatures with increased Zener pressure and solid drag, the residual deformation (or dislocation density) is transferred into the next pass more effectively. It is also recognized that in the finishing stage the microstructural evolution is complex as partial softening could also be present. Highest accumulated strain throughout the successive per-pass reductions is to be found during the finish rolling, affecting the dislocation density, ρ. If a recrystallization fraction of 5% or lower is taken as a definition for achieving the non-recrystallization region (under T_{nr}), based on MicroSim predictions, this is accomplished only by one schedule with the slab reheating at the lowest temperature, at 1180 °C, and by considering other parameters close to constant. This schedule was also used for industrial testing with and without introduced Nb.

The influence of decreased slab temperature on decreased recrystallization kinetics in the plate was briefly discussed, and when introducing the Nb under the lowest slab temperature, an additional retarding effect is observed (see Figure 2). The change is attributed to the presence of low-density homogeneous precipitated secondary Nb-based particles under 1167 °C, predicted by Thermo-Calc (see Figure 3), and due to the Nb present in the solid solution of austenite that is partially segregated into the grain boundaries, causing the so-called solid drag [35]. It is assumed that increased solid drag, when Nb is introduced, is (among other roughing passes) present mainly during the last roughing passes. Solid drag and interaction of simultaneous precipitation of heterogeneous Nb-based particles in the finishing stage additionally decrease the grain mobility and grain boundary movement due to effective Zener pinning force where growth and coarsening phenomena are also present (Figure 2). Taken from [35], the recrystallizing austenite growth rate $\dot{D}_{\mathrm{r}x}$ is related to the change in effective high angle grain boundary (HAGB) mobility, $M_{\mathrm{eff,HB}}$, as a part of solid drag and precipitation (M_{prec}, M_{SD}) even if a similar driving force, P_{D}, for SRX exists, due to comparable rolling schedule and affecting the dislocation density. Both nucleation rate, $\dot{N}_{\mathrm{rx}}$, and $\dot{D}_{\mathrm{r}x}$ have an influence on the evolution of the time-dependent recrystallization fraction, $\dot{X}_{\mathrm{r}x}$ observed in Figures 1 and 2.

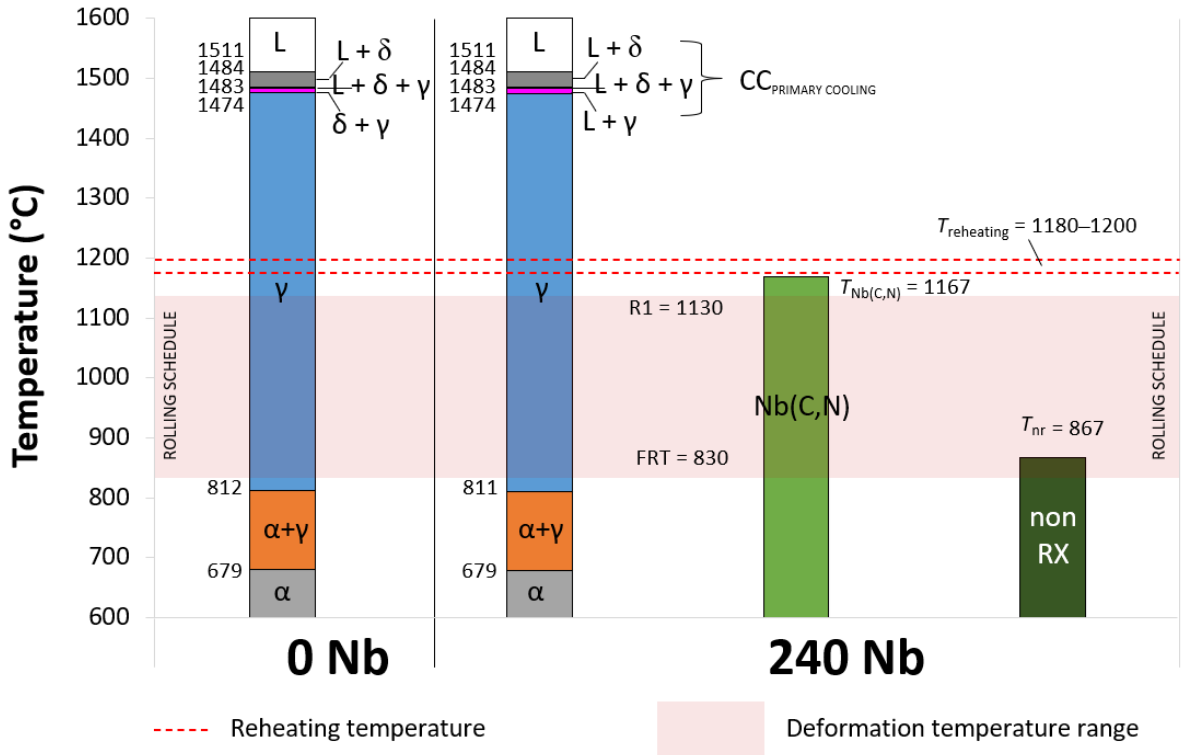

Figure 3. Equilibrium thermodynamic determination of phase stabilities of investigated C-Mn samples, using Thermo-Calc. Both compositions, 0 Nb and 240 Nb, have the same rolling window related to the temperature austenite existence.

3.3. Thermodynamic Prediction

Figure 3 shows a simplified presentation of the phase evolution of equilibrium solidified 0 Nb and 240 Nb samples by including only major phase constituents. Based on predictions for 240 Nb, Nb(C,N) is stable under 1167 °C if Thermo-Calc is considered. If the calculation is performed according to Irvin et al. [36], the temperature is similar to 1175 °C. This means that the majority of the roughing phase for 240 Nb is already in the region of thermodynamically stable precipitation of small amounts of Nb(C,N). Effective strain-induced precipitation is expected under 867 °C determined by the semi-empirical equation for T_{nr} [37]. The results of all characteristic temperatures are gathered in Table 2. FRT for 0 Nb and 240 Nb was estimated to be in the region between 880 and 830 °C. Both temperatures are above A_{r3} at 758 °C if the equation in [38] is considered as a function of plate thickness. This is also above A_{e3} at 811 °C if Thermo-Calc is considered (Figure 3). The last per-pass reduction is still completed in the austenite region. Under approximately 703 °C, cementite carbides are also stable as a part of the eutectoid reaction. The latter is not shown for easier graphical visualization. The comparable liquidus and solidus temperatures, T_{liq} and T_{sol}, indicate a similar elemental segregation tendency during CC based on Table 1. All other parameters are taken as nearly constant during CC slab production with comparable achieved internal quality determined by macro-etched samples extracted from the strand. A similar internal quality of the as-cast state and solidification history should be considered for limiting potential variation of measured mechanical properties, such as low-temperature toughness measurement. However, based on [39], the addition of Nb under non-equilibrium conditions can promote the formation of coarse Nb-based eutectics during slab production as shown in [40], degrading through-thickness properties according to EN 10164 [40,41]. As this is related to control of excessive segregation by control of basic chemical composition, solubility product [M] [X], CC parameter adjustments, etc., the prevention of excessive segregations and potentially deleterious influence of the coarse formation of Nb(C,N) eutectic clusters on the final plate functionality in the context of arc

welding and oxy-fuel plate cutting is not discussed in this paper, being outside of its scope. However, when shrink porosity is present due to solidification history, regardless of Nb addition, and by using a rolling schedule with restricted stored energy of deformation as studied in this paper, the penetration depth is highly limited to weld those defects which are then observed under ultrasound testing (UST) of a final plate. In the case of conducted industrial trials, no UST indications on final plates (0 Nb and 240 Nb) were recognized.

Table 2. Characteristic temperatures and austenite and ferrite grain sizes after phase transformation.

Test	Predicted—PAG					Measured—FG			
Sample	T_{NbC} (°C)	T_{NbC} (°C)—Irvine	T_{nr} (°C)	G_{Avg} * (µm)	G_{Max} * (µm)	**Direction**	G_{Avg} (µm)	G_{Max} (µm)	G_{Avg}/G_{Max}
0 Nb	-	-	790	43.6	205	Transverse	22.2	61.5	0.36
						Longitudinal	22.0	67.8	0.32
240 Nb	1167	1175	867	28.8	150	Transverse	16.1	56.9	0.28
						Longitudinal	16.5	54.5	0.30

* Predicted after final F4 pass—completion of hot deformation.

As discussed, the slab reheating temperature (1180–1200 °C) marked with a red discontinuous line in Figure 3 is predicted to be above equilibrium precipitation of homogeneous Nb(C,N) from austenite, calculated by Thermo-Calc. Precipitation of secondary particles, described as Nb(C,N), is under T_{sol}. This means that under close to equilibrium solidification (Lever rule), no Nb-based eutectics are expected. Based on Thermo-Calc calculations, the first roughing pass is already under the solubility temperatures of Nb(C,N) in austenite, and the maximum volume fraction potential for homogeneous (down to T_{nr}) and combined homogeneous–heterogeneous precipitation (down to T_{nr} and to or just under FRT) is in the range of 2.7×10^{-4} and 1.0×10^{-3}, respectively. This is within the limits for C-Mn steels [1,42]. In the case of sample 240 Nb, the last finish passes are performed in the region of heterogeneous nucleation of Nb(C,N), under T_{nr}, for effective grain boundary pinning, as also shown in Figure 3. Based on the Ashby–Orowan relationship, if effective (5–10 nm) particle size is considered for 240 Nb [1], then precipitation strengthening should be in the range of $\Delta R_{p0.2} \geq 30$ MPa and limited to 90 MPa. The lowest $\Delta R_{p0.2}$ value is related to volume fraction related mainly to homogeneous precipitation of Nb(C,N).

3.4. Hot-Deformation Behavior—Penetration Depth

Based on the FEM model, the through-section extent of true strain ε, and stress was predicted on the actual rate of deformation $\dot{\varepsilon}$, average cross-section temperature T (approximate linear cooling [5]), per-pass reduction for exit height H, engineering reduction e_H, etc. The physical data were obtained from the Gleeble tests ($\sigma - \varepsilon$ curves at constant T and $\dot{\varepsilon}$) and from JMatPro (such as temperature-related density). In Figure 4a, a representation of non-homogeneous stress distribution inside the effective deformation zone is shown (in Pa) as a consequence of temperature-dependent material characteristics and kinematic settings ($\dot{\varepsilon}$, ε, T, etc.) from R1 to R7. It is obvious that according to Figure 4a,b, the stress uniformity increases with the last roughing passes, similar to that observed in the case of equivalent strain, where uniformity increases with increased per-pass reduction and control of work roll rotation speed [24]. However, the strain distribution is usually more stable as related to rolling parameters than stress as related also to material characteristics and therefore reveals the true nature of rolling complexity under low energy deformation rolling schedule and the unstable austenite conditioning degrading the needed mechanical properties.

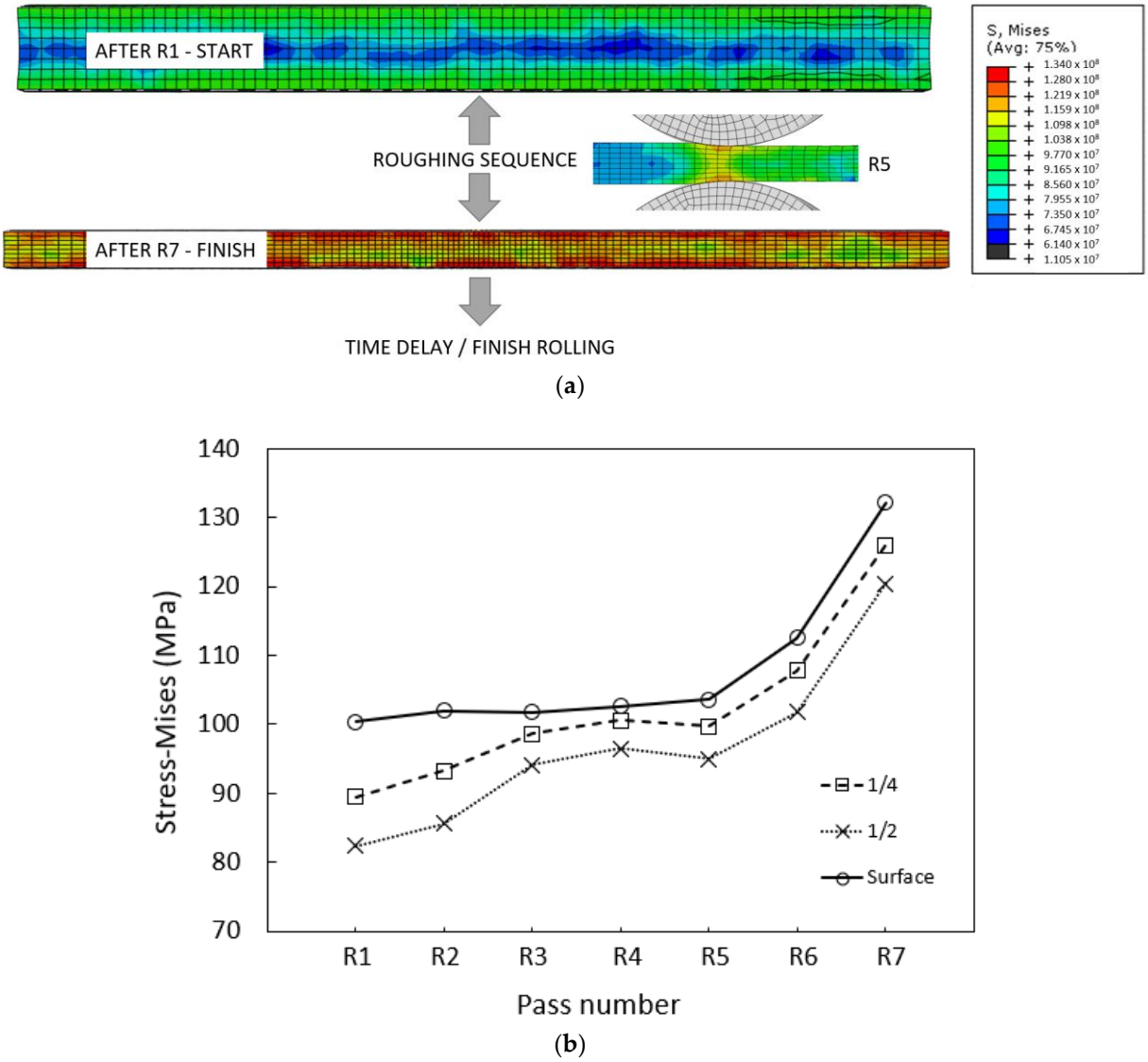

Figure 4. (**a**) FEM simulated effect of rolling schedule on through-thickness non-homogeneous stress distribution (from surface to center). The cross-section is taken mid-length of the plate. (**b**) Stress variation determined at the highest stress levels inside the effective rolling region shows an obvious change in the cross-section deformation efficiency and related dislocation density due to not only the change in temperature-dependent material characteristics but also the change in work roll-speed rotation as in the case of R6 and R7 (with comparable per-pass strain).

3.5. Mean-Flow Stress Curves

Based on [18,23], three basic recrystallization–deformation behaviors are recognized: static recrystallization (Type I); unwanted partial recrystallization (Type III) defined between RST and RLT (due to interaction of austenite continuous grain growth, pinning of PAG, and nucleation of new dislocation free grains), or simply the region of T_{nr}; and region of no recrystallization, below RST or T_{nr} (Type II). All deformation behaviors are listed in Figure 5a. The estimated regions are based on the values taken from [23]. The latter is related to Nb microalloyed 240 Nb sample only. Based on the methodology in Figure 5a, no remarkable deformation in Type III was present. Therefore, the fine-to-coarse grain distribution structure interpreted originates mainly from the roughing stage.

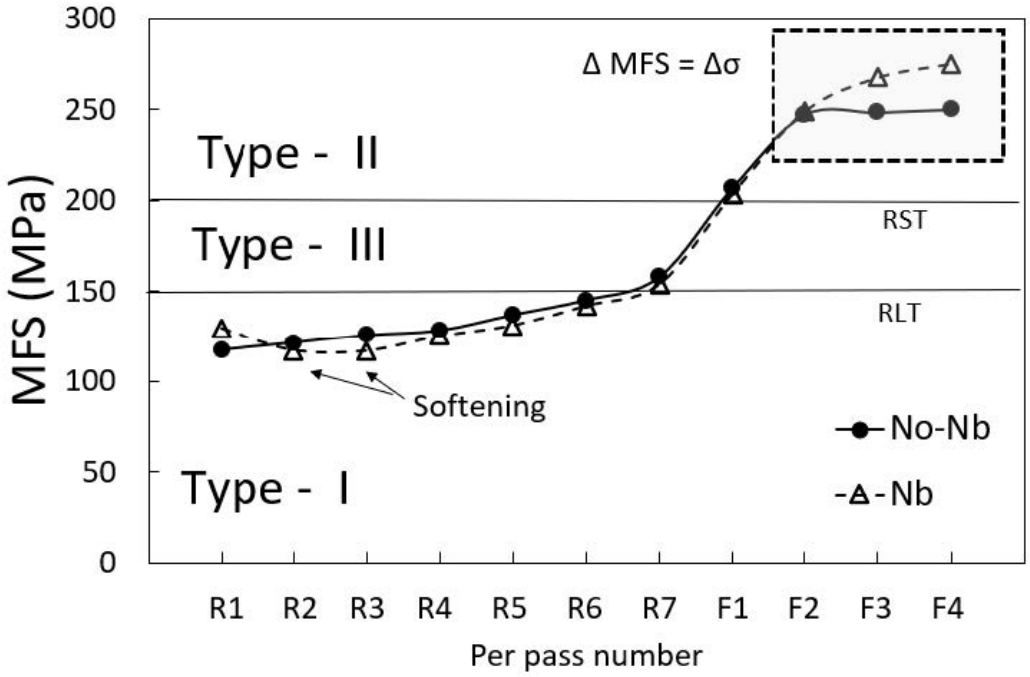

(**a**)

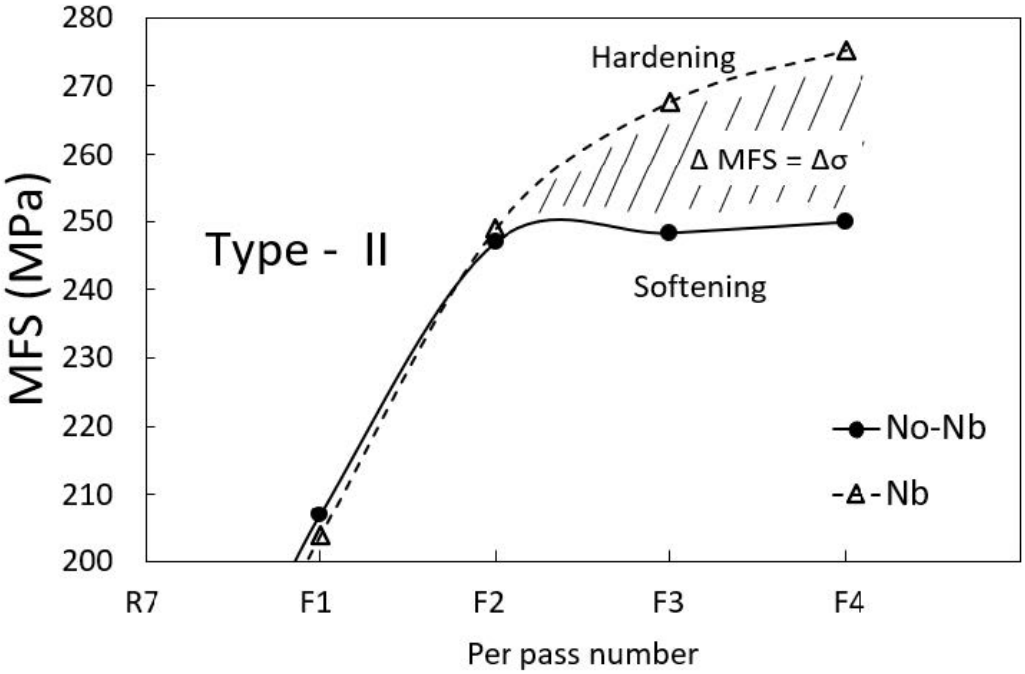

(**b**)

Figure 5. *Cont.*

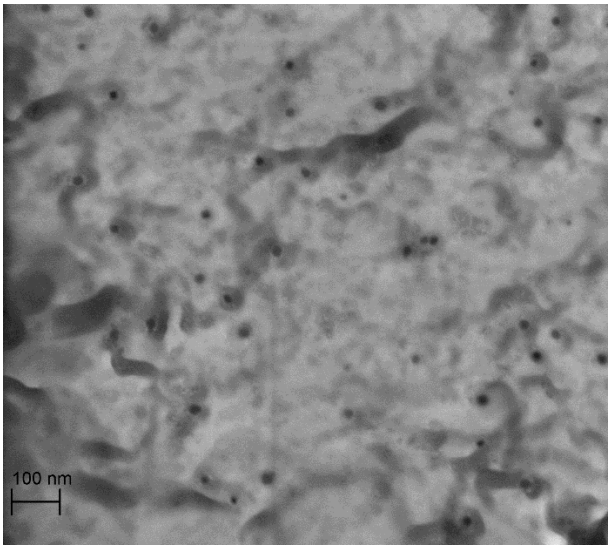

(**c**)

Figure 5. Evaluated MFS from the measured rolling force for steel 0 Nb and 240 Nb. (**a**) MFS during the complete rolling phase in austenite region. (**b**) MFS detail on final reductions. In the case of 0 Nb, the rolling is performed only in the Type I region as T_{nr} is below FRT, see Table 2. (**c**) STEM visualization of small (dark) nanosized particles of Nb(C,N), randomly distributed, observed on a carbon replica in average size of 8.2 nm with a maximum sized up to 16.3 nm for 240 Nb. Accelerating voltage: 30 kV.

Starting MFS is similar for both samples under the same rolling schedules and due to the similar base chemical compositions, reheating slab temperatures, slab temperature drops before R1, etc. Almost periodic variation of the MFS curve in the roughing phase is observed for 240 Nb. This is an indication of possible effects of locally finer initial PAG size (Nb is considered as an effective grain size controller also during slab cooling and slab reheating before hot rolling) and/or simultaneous progressive grain coarsening and potential lengthening of the recrystallization nucleation time compared to stable stress flow observed for 0 Nb. This means, if the analogy is taken from [5,43], certain grain size heterogeneity in the roughing stage from MFS observation is expected for 240 Nb, if considered that unstable rolling is present, $\varepsilon \ll \varepsilon_{cr}$, where ε_{cr} is interpreted as needed real deformation for a single and full recrystallization wave per pass. The delayed softening for 240 Nb presented in Figure 5a and according to Figure 2 is interpreted due to increased pass-to-pass accumulated strain compared to 0 Nb. The interpass times, defining the softening intensity or potential ability for achieving a certain SRX fraction between passes, were maintained the same for both compositions.

The value of MFS for the first finishing pass (F1) indicates a reproducible starting point for the finishing rolling stage related to a reproducible temperature drop resulting from the chosen time delay between the last roughing pass, R7, and the first finishing pass, F1. The MFS curve in the type II region differs considerably between 0 Nb and 240 Nb with close to constant ε, $\dot{\varepsilon}$, and t for both samples in the last rolling phase. The latter indicates the absence of intense recrystallization and increased accumulated strain as well as precipitation hardening for 240 Nb (Figure 5b,c). This means that different recrystallization kinetics are present when Nb is added regardless of the presence of partial SRX in the roughing phase, if MicroSim and MFS values from experimental tests are considered. The slope of MFS as an indicator of the intensity of dispersion hardening is estimated to be less emphasized at the last deformation pass and lowest per-pass temperature, such as at F4 (being close to FRT), partially due to the limited dissolved [Nb] left in austenite but also due to partially refined PAG in the roughing stage and weak successive ε in the finishing phase, as it is recognized that deformation enhances the precipitation kinetics [15]. This also affects the final FG refinement after $\gamma \rightarrow \alpha$ phase transformation [12].

Based on the MFS curves from Figure 5 and information about σ_y obtained from the Gleeble hot-compression tests, a simplified prediction of potential maximum allowable dislocation density, ρ, using the highest stress values determined at F4 in Figure 5 was made. The estimation for 0 Nb and 240 Nb, if hardening is the main mechanism, is under 1.1×10^{15} m^{-2} and 1.5×10^{15} m^{-2}, respectively, being close to similar values reported from [15] or [35]. The calculation procedure can also be found in [25]. However, this is informative only as XRD is usually performed in relation to FRT [42]. This means that changes observed on MFS as an effect of Nb addition for 240 Nb are possible due to allowable nucleation sites N_0 for Nb(C,N) estimated to be in the range of 2.7×10^{22} m^{-3} if Equation (1) is considered. The dislocation density is lowered under slow cooling of the plate. The presence of small nano-sized particles (presumably Nb(CN)) in the final as-rolled state was noticed and is seen in Figure 5c; they were not observed in the 0 Nb samples. The identification of such particles as Nb(C,N) by using similar nominal steel compositions can be seen in [25]. Precipitation of Nb(C,N) potentially slows down the dislocation annihilation, and this increases the number of dislocation–particle interaction sites as the particles can also work as a generation source for increasing the dislocation density in 240 Nb.

3.6. Microstructure

In Figure 6, microphotographs taken at the same magnitude show a ferrite–pearlite microstructure banding with no visible bainite formation or coarse acicular structures that could potentially affect final mechanical properties. In both cases, alternate bands of ferrite and pearlite are detected without pancaking due to rather limited accumulated strain and final plate exit thickness, meaning that equiaxed PAGs were mainly present before $\gamma \rightarrow \alpha$ transformation. Etching response is more emphasized for the microstructure of a sample microalloyed with Nb, indicating the presence of finer lamellar structure of pearlite. Details of a secondary phase can be seen in Figure 6c,d. Based on Figure 6a, low-temperature products also seem to be formed; however, based on the SEM analysis, this was not confirmed, as stated above. A small fraction of bainite, according to the CCT diagram, is not excluded for the Nb-based sample, especially if heavy centerline elemental saturation is present resulting in coarse Nb(C,N) affecting also PAGS. Coarse Nb(C,N) was not observed in the 240 Nb. As mechanical properties are mainly defined by polygonal FG size and ferrite content, a quantitative analysis using ImageJ was performed. The pearlite content for 240 Nb and 0 Nb was measured at 42% and 37%, respectively. This can influence the final mechanical properties to a certain extent. The average grain size G_{Avg} was used to estimate the potential change in R_{m}. It is recognized that Nb addition influences the ferrite and pearlite regions inside CCT diagrams, and therefore some change in pearlite fraction is possible [1]. In our case, rather small changes are expected if no extensive elemental segregation is present (among rather small G_{Avg} deviation between both samples); therefore, the small change in areal fractions could also be related to cross-section cooling rate variation (see Figure 6e).

3.7. Grain Size Evolution

3.7.1. Prediction

Grain size evolution was observed with MicroSim by setting the initial grain size distribution, composition, and related rolling schedule according to SRS. Three schedules (at reheatings of 1180, 1230, and 1280 °C) for Nb-based samples (240 Nb) were simulated and one additional for non-microalloyed composition (0 Nb) at a chosen lower slab temperature of 1200 °C. For this study, the initial PAG distribution was kept the same for all reheating temperatures with G_{Avg} = 150 µm and G_{Max} = 450 µm as a starting point of non-deformed austenite. Considerable grain growth can appear at the highest slab temperature for the 240 Nb sample, regardless of the use of Nb, as the solid drag influence is lowered with temperature increase, and grain and subgrain mobility is increased (Figure 7a). This starting slab grain growth phenomenon is also affecting the achievable final average PAGS

where presumably secondary grain growth appears during the time delay between R7 and F1 resulting from a close-to-linear temperature increase. This is reasonable due to the lack of pinning elements, such as TiN [44]. In this study, the titanium content is measurably far below 0.01% in the current alloys. In Figure 2, sample 240 Nb reveals increased solute drag (SD) and therefore altered grain boundary mobility, M_{SD}, on existing driving pressure for SRX, P_D, in the roughing stage. Mo is not taken as decisive due to very limited and comparable content for both samples (0.05 and 0.04 mass % in 0 Nb and 240 Nb, respectively). As discussed above, an incomplete recrystallization fraction was predicted for both compositions.

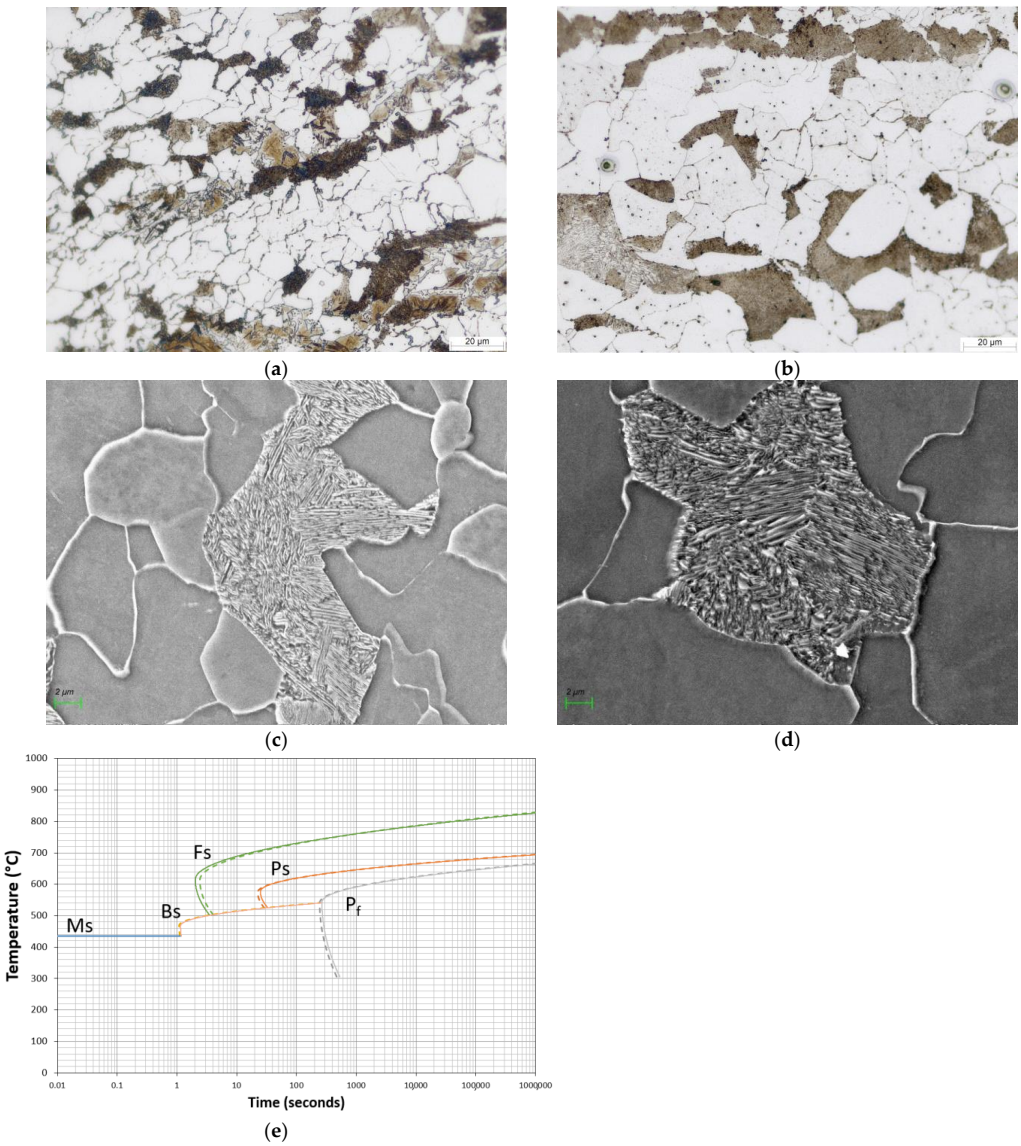

Figure 6. LOM: (**a**) with Nb (240 Nb) and (**b**) without Nb (0 Nb). Etchant: Nital 4%. Enlargement: 500×. Observation: perpendicular to the main rolling direction. FE-SEM using SE2 detector: detail of typical secondary phase (within pearlite) in the (**c**) 240 Nb sample and (**d**) 0 Nb sample. Enlargement: 8000×. (**e**) Predicted CCT based on internal experimental database with Nb (dashed line) and without Nb (full line) and non-deformed PAG.

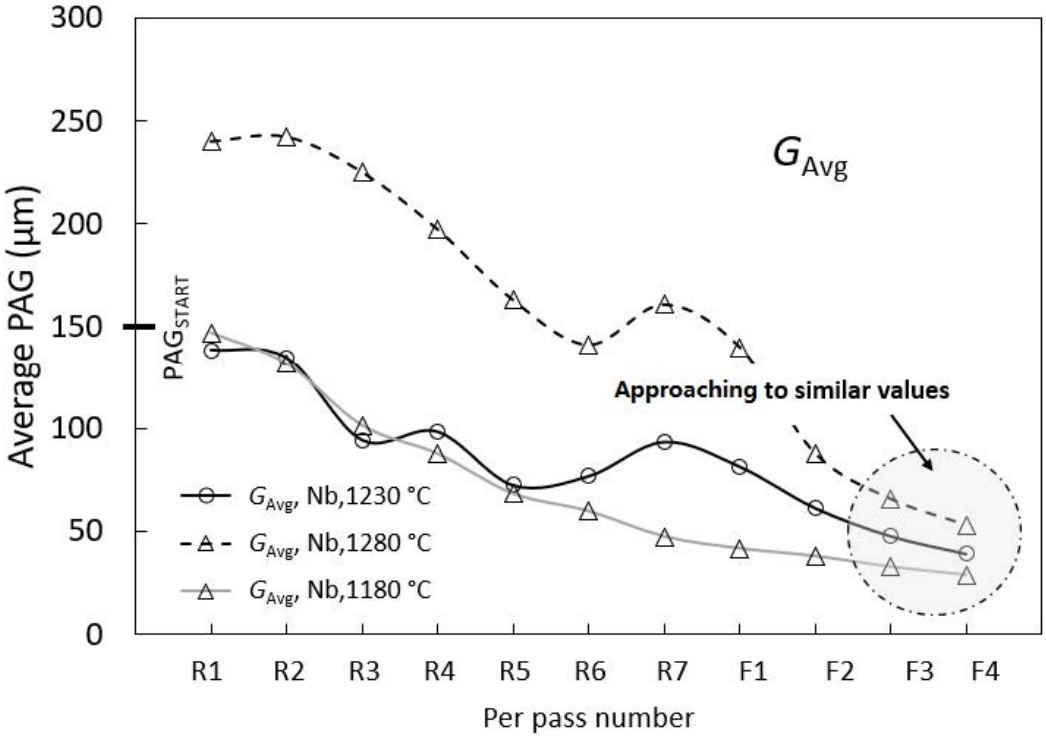

(**a**)

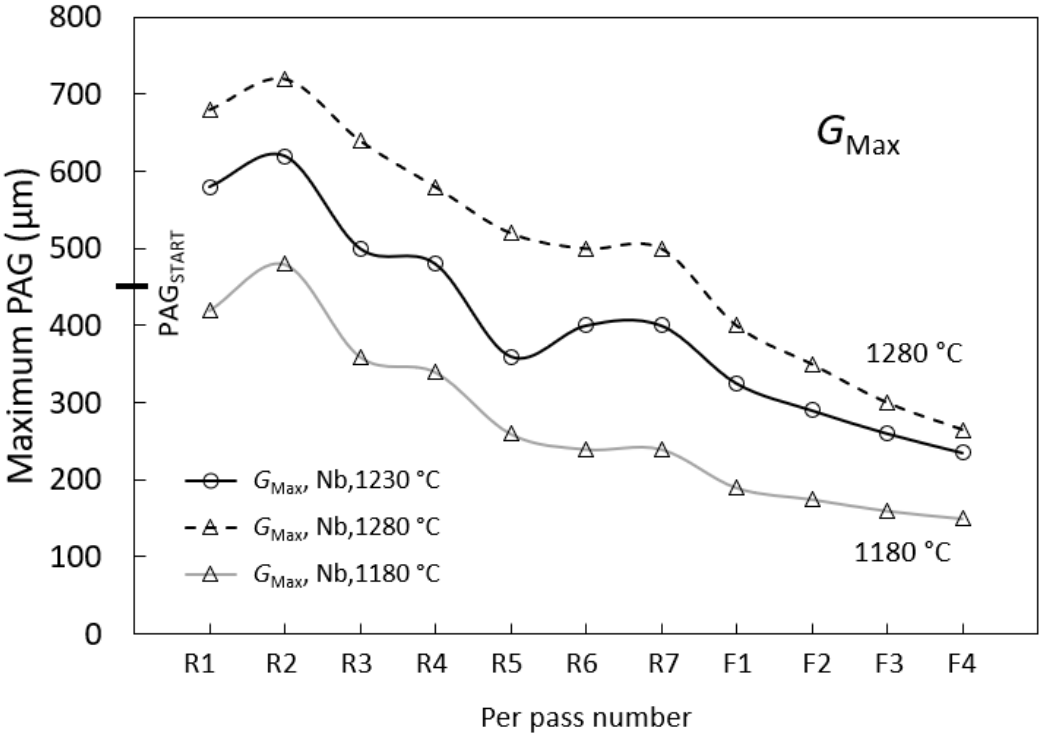

(**b**)

Figure 7. *Cont.*

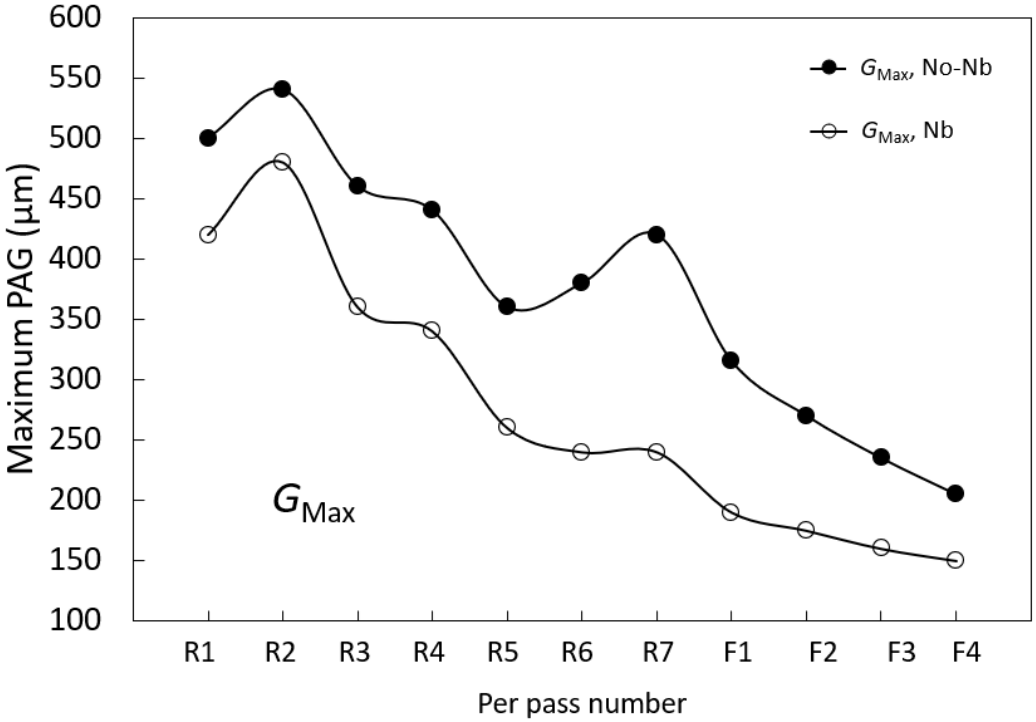

(**c**)

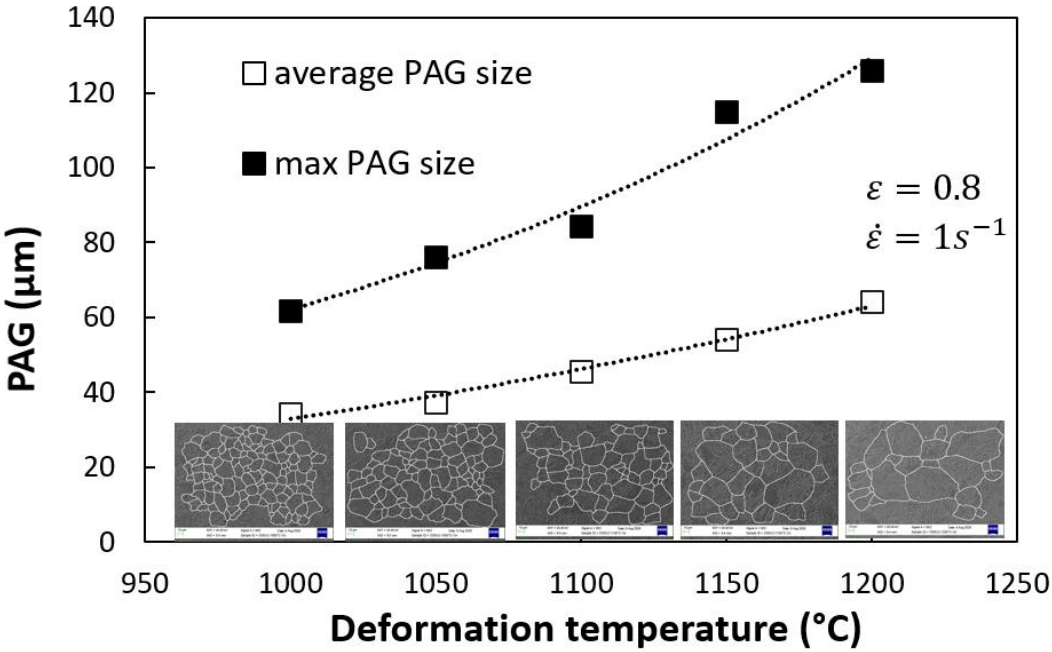

(**d**)

Figure 7. High-temperature (SRX) grain size evolution predicted with MicroSim: (**a**) Influence of reheating temperature on average PAG and (**b**) the variation of maximum PAG distribution. (**c**) Influence of added Nb on maximum PAG at lowest reheating temperature (1180–1200 °C). (**d**) Lower limit G_{Avg} and G_{Max} as a function of deformation temperature at fixed low strain rate 1 s^{-1} and high per-pass strain, $\varepsilon = 0.8$, determined using thermomechanical simulator Gleeble 1500D for up to 0.01% Nb.

An overall grain refinement is observed during rolling, and G_{Avg} evolves to similar values regardless of the PAG starting condition and despite predicted changes in SRX kinetics due to the unstable roughing phase with and without the introduction of Nb. Slab

reheating temperature and Nb addition (240 Nb compared to 0 Nb) majorly influence G_{Max} values. Under the unstable roughing phase, the considerable variation of slab temperature is therefore influential for grain size distribution and potential variation of mechanical properties related to the effective grain size. This also indicates the importance of slab production with previously defined starting PAG distribution. With increased per-pass reductions with fewer passes, the starting PAG is becoming less influential as similar G_{Avg} is obtained earlier, under the first several roughing passes, as indicated with hot rolling simulation experiments in [12]. In Figure 7c, a comparison is made between G_{Max} for both compositions (with and without Nb) with evident susceptibility for secondary grain growth for 0 Nb under similar temperature regimes between time delay and therefore affecting the final coarsest grain size defining final ductility properties. This agrees well with [12,45], meaning that Nb acts as a stronger recrystallization delaying element (compared to Ti, V), which leads to grain refinement even under such variable rolling conditions with insufficient static recrystallization when executing the last finishing passes at sufficiently low temperatures. An example of intensive continuous PAG refining under a heavy roughing regime from 1200 to 1000 °C for C-Mn steel is shown by the constructed diagram in Figure 7d for G_{Avg} and G_{Max} obtained from Gleeble hot-compression tests where approximately 35 µm was set as the ultimate lower PAGS and surprisingly close to the G_{Avg} obtained for lowest reheating slab temperature (1180 °C) and Nb addition at R7 in Figure 7a. However, the G_{Max} regardless of reheating slab temperature is much higher than the limit for the roughing phase with G_{Max} = 61 µm at $\varepsilon = 0.8$ and $\dot{\varepsilon} = 1s^{-1}$, showing the importance of including the grain size distribution into the regular inspection of a plate rather than using infrequent average grain size results as it is obvious that similar G_{Avg} and therefore similar G according to ASTM E112 can have considerable variation in measured mechanical and functional properties especially important for unstable rolling as shown in the particular study.

3.7.2. Measured Grain Size

A cross-sectional FG size was evaluated on samples extracted from the heavy plates by considering more than 1000 grains measured in longitudinal and transverse directions compared to the main rolling direction for direct comparison of Nb efficiency having unstable rolling with incomplete austenite recrystallization in the roughing stage. Regardless of the rolling direction, the microstructure formed after cooling is refined by using Nb (Figure 8a,b). Both samples have asymmetric distribution frequency of grain size, and importantly, multimodality is observed on both grades, an indication of an unstable roughing process (see black arrows in Figure 8a,b).

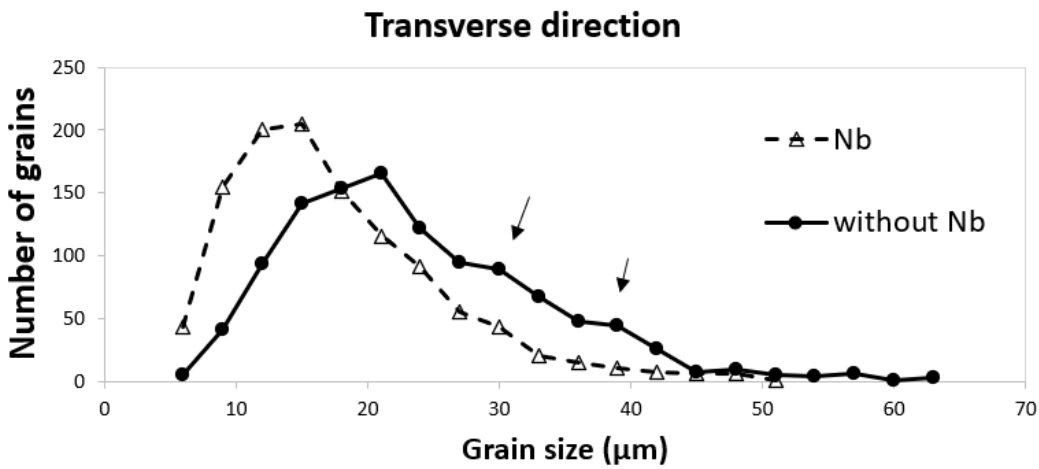

(**a**)

Figure 8. *Cont.*

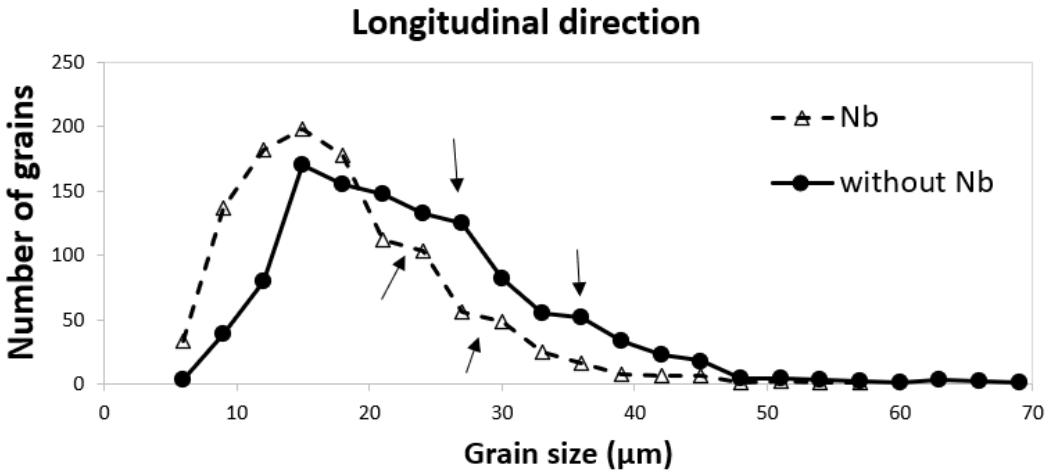

(**b**)

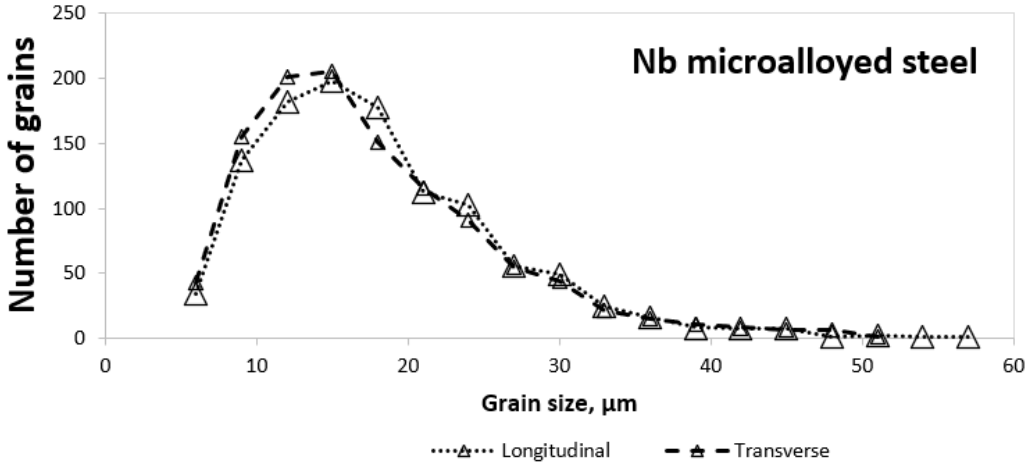

(**c**)

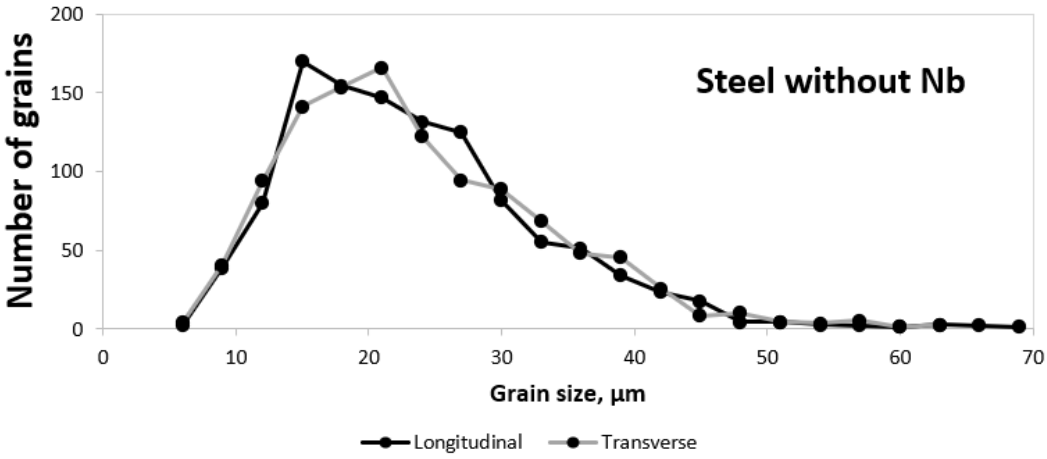

(**d**)

Figure 8. Frequency distribution of FG size evolution for 0 Nb and 240 Nb: (**a**) transverse (T) and (**b**) longitudinal direction (L). (**c**) An FG comparison evolution based on the T-L directions for 240 Nb. (**d**) An FG comparison evolution based on the T-L directions for 0 Nb.

As described in [22], it is obvious that PAGS defines final FG size, and the Nb microalloyed sample is measurably refined in the current study compared to base composition regardless of non-uniform deformation phenomena presented by the FEM simulation. By comparing the average PAGS after F4 and average final FG size in the final microstructure, the reduction factors for $\gamma \rightarrow \alpha$ transformation for the current study are estimated to be similar, within 1.96 for 0 Nb and 1.70 for 240 Nb. These values can be used for reconstructing PAGS for other similar rolling schedules. Both factors are close to the correlation between ferrite and austenite grain size for C-Mn steel [12].

Figure 8c,d reveal no excessive anisotropy in grain size distribution if preferential directions are considered, and therefore the anisotropy related to the main rolling direction is taken to be low. If the distribution factor is considered, defined as G_{Avg} to G_{Max} ratio, the enhanced anisotropy is however measurably higher for 240 Nb with a factor of 0.29 compared to 0.34 for 0 Nb. This could also be an indication of a possible increase in the scatter of measured mechanical properties when Nb is introduced under such an unstable rolling condition.

The results in Figure 8 are in very good agreement with predicted PAG evolution after all executed deformations (F4) in Figure 9 where Nb addition is recognized to have modest influence as in the case of FG with obvious multimodality regardless of Nb addition.

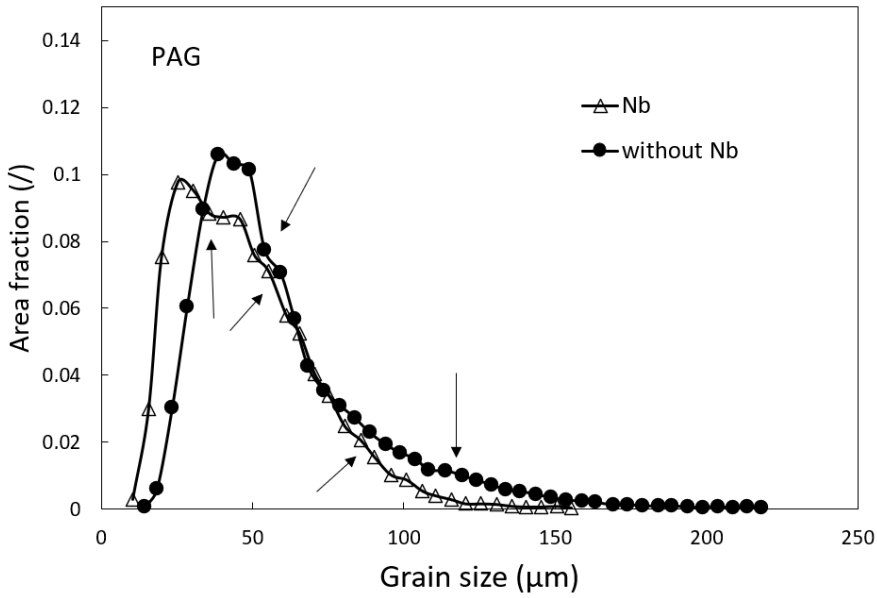

Figure 9. Frequency distribution of predicted PAG with obvious multimodality (highlighted with arrows).

3.8. Mechanical Properties in as-Rolled State

As shown in [22], the stability of the Charpy energy is greatly affected by the change in the metallurgical reduction ratio. In the presented paper, the total metallurgical reduction ratio was kept the same within the same basic composition for both processed plates to limit variation in parameters. It should be emphasized that the (roughing) rolling temperatures for this particular study were kept outside the region of sluggish recrystallization (above RLT or RST) that can lead to variable results of mechanical properties for Nb microalloyed steels [1,45]. Different factors contribute to the strength (R_m), such as solid-solution hardening, pearlite percentage, ferrite grain size (Hall–Petch), effective dispersion hardening, and dislocation density [33,36]. The obvious change due to the addition of Nb when considering the variable rolling conditions is observed in the change in (finer) average $G_{Avg,}$ and the changed distribution factor G_{Avg}/G_{Max} is also a measurable effect of strain-induced precipitation observed after a change in MFS as guidance of metallurgical behavior with evidence of nanosized Nb(C,N) (detected using STEM) working as a retarding force on the grain

boundary. The predicted tensile strength changes between 0 Nb and 240 Nb are based on the Pickering equation taken from [29] and are estimated to be in the range of 25 MPa. The measured average yield strength (observed by $R_{p0\cdot2}$ instead of R_{eH}) is detectably increased for 24 MPa for the Nb-added sample (Figure 10). Combined Ashby–Orowan precipitation and Hall–Petch refinement strengthening should be considered as a contributor as this phenomenon was published already in the early papers of Nb testing under various rolling schedules, despite rolling fluctuations, FRTs, and final thicknesses [1,5]. This also means that if the same rolling schedules are used (with the same nominal Nb percentages) and a considerable scatter of yield strength is achieved for the same nominal plate thickness, a considerable temperature profile variation, starting from the reheat slab temperature to FRT, should be considered. Temperature changes influence interphase NbC precipitation considerably (if FRT is high enough) by influencing particle size, density, and pining capability as well as partially changing the volume fraction of transformation products. Less change was measured for R_m with a 13 MPa increase with Nb addition (also based on similar C, Si, and Mn and comparable pearlite content), and almost negligible change was measured for A_5 with a 1.2% increase in favor of Nb microalloyed steel. This means that the most promising change and enhancement are notable for $R_{p0\cdot2}$ when Nb is introduced regardless of incomplete recrystallization in the roughing stage. However, it should be remembered that quite average Nb addition was also used (240 ppm). Low-temperature toughness (ISO-V) is, despite similar A_5, measurably higher for Δ = 32 J on average for 240 Nb. Here, it should also be remembered that refining and precipitation hardening can have a combined effect; therefore, the evaluation of potential toughness decrease or increase based on $R_{p0.2}$ scatter is not recommended as virtually the same strength values can give considerably different toughness values [5]. The absolute toughness range defined between min. and max. ISO-V is increased compared to the base 0 Nb composition and agrees well with the less favorable distribution factor G_{Avg}/G_{Max} detected for 240 Nb. For both compositions, a single average toughness value, a so-called outlier, was also under the minimum demand of 27 J at 12 and 25 J for 0 Nb and 240 Nb, respectively, revealing the major negative influence of low deformation energy rolling strategy with incomplete SRX on ductility properties (marked with a star, Figure 10). This means that the grade is not classified as J2 quality. According to [33], most of the toughness and elongation (ductility) are attributed to grain size distribution, and an increase in ductile-to-brittle transition temperature (DBTT) is related to precipitation hardening and to microstructure/grain heterogeneity. Based on the data in Figure 10, the achieved low-temperature values are still moderate for both steels. Using the embrittlement vector (-0.7 °C MPa^{-1}) for grain size variation [5], the potential decrease in DBTT is up to a moderate -16.8 °C when Nb is introduced and confirms the measurable but moderate influence of grain refinement phenomena measured in Table 2.

Considering normal cumulative distribution factor (CDF), it is recognized that the probability for Charpy measurements to be under the prescribed limit, according to EN 10025-2 [28], is severely decreased if Nb is introduced, and this is changed from 31.8% to 9.1%. This also applies for elongation, A_5, with a probability change from 16.4% without Nb to only 2.4% with added Nb according to the prescribed minimum values [28]. It should be emphasized that these values are purely informative due to the limited amount of data. Therefore, the produced grade under the variable conditions with low stored energy rolling schedule is equivalent to the quality of nominal yield strength of 355 MPa. For higher classes such as 460 MPa (with min. 420 MPa between 40 and 63 mm), the rolling schedule and therefore the yield of Nb including the cooling regime is not considered to be optimal for the given composition. This indicates that such instabilities, described as incomplete SRX in the roughing phase, are partially excluded only for lower strength grades with lower ductility demands (J0) and rather high total metallurgical ratios (lower exit thicknesses).

All obtained results indicate that under variable rolling conditions, the variation of mechanical properties indicates a need for increased sampling, and this seems to be more enhanced with Nb addition, for the same steel grades, quality, and delivery condition for comparable thickness. This means that under a low deformation energy rolling schedule,

the Nb addition can even increase production instability, especially if heavy plates are considered. Under such a production condition, the position of extracting ISO-V samples should be moved towards the center of the plate. Currently valid standards, such as the standard for hot-rolled structural products described in EN 10025-2 [28], may therefore be limited for such unstable plate production.

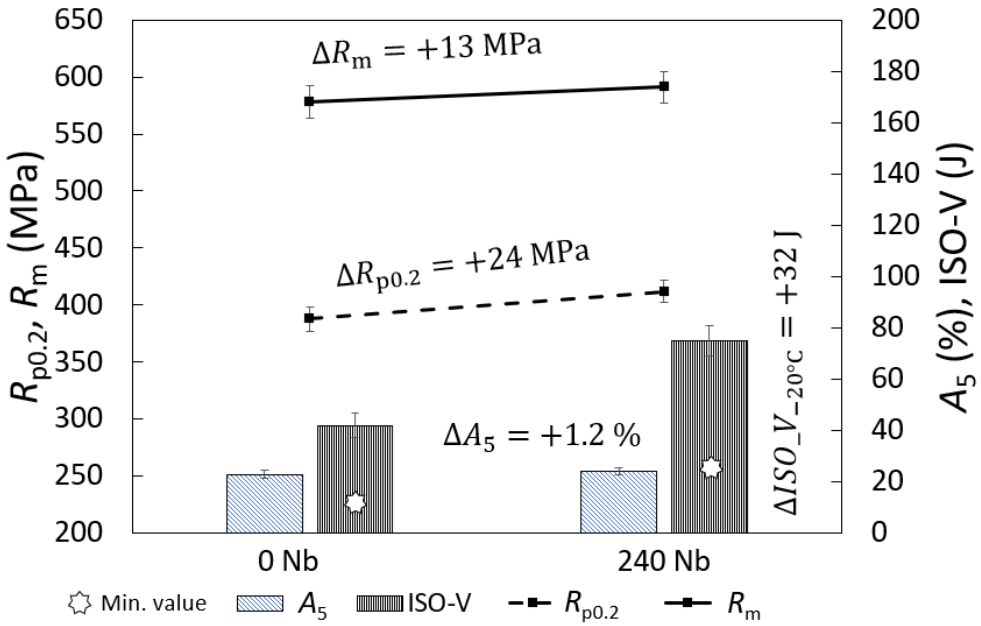

Figure 10. Tensile strength and transverse low-temperature toughness properties (−20 °C) for 0 Nb and 240 Nb in as-rolled state after partial SRX in the roughing phase. Outliers for toughness are marked with star signs.

4. Conclusions

A good correlation of Nb efficiency between prediction and experimental work has been achieved with regard to grain size evolution that affects the ductility properties. The starting slab temperature and the previously defined starting grain size distribution under variable roughing conditions have an enhanced and logical role in evolved PAG and FG size and distribution. By implementing lower slab temperature reheating for low energy deformation rolling, successful production of a rather fine-grained Nb-based constructional heavy plates is still achievable, but the process itself can be non-repeatable due to the non-optimal roughing stage defined with low per-pass reductions, short interpass times, and other parameters. The influence of Nb was still measurably demonstrated even when considering the variable roughing condition by considering MicroSim, MFS, FG size distribution with observed multimodality, and measured mechanical properties for the given rolling schedule. Incomplete SRX and limited total metallurgical reduction can have an important impact, not only on a reduced Nb efficiency, but also on the potentially increased scatter of the mechanical properties. Using FEM, an inhomogeneous cross-section stress distribution from the surface to the center of the plate thickness during the entire low energy deformation roughing stage was strongly exhibited. This was subsequently indicated on the cross-section PAG variations. It is evident that when Nb is implemented under such conditions with incomplete SRX, the ductility values determined by the low-temperature toughness and ductility can be increased on average. However, the range of the measured toughness values can also be increased by an enhanced degree of anisotropy in the case of the Nb addition. This reveals the important aspect of the problematic uncertain specific interpretations of Nb contribution under variable plate production and on the use of the current production standards for the evaluation of C-Mn steel plates, where sample extraction positions are usually prescribed in the region outside where the highest

instabilities can be formed during the hot plastic-deformation in the roughing stage, and these may affect the final plate characteristics.

Author Contributions: Conceptualization, G.K.; methodology, G.K. and J.F.; software, P.L. and U.K.; validation, G.K., B.B. and J.F.; formal analysis, G.K.; investigation, G.K., J.F. and M.K.; data curation, G.K.; writing—original draft preparation, G.K.; writing—review and editing, U.K., P.L. and D.S.; visualization, G.K. and U.K.; supervision, G.K. and P.L.; project administration, B.B.; funding acquisition, B.B. All authors have read and agreed to the published version of the manuscript.

Funding: This research was supported by SIJ Acroni, d.o.o., Slovenia.

Data Availability Statement: Not applicable.

Acknowledgments: The authors would like to acknowledge the CBMM team for constructive discussions about Nb usage in carbon steel plate manufacturing. We would also like to acknowledge the University of Ljubljana, Faculty of Mechanical Engineering, Aškerčeva Cesta 6, 1000 Ljubljana.

Conflicts of Interest: The authors declare no conflict of interest. The funding sponsors had no role in the choice of the research project; the design of the study; the collection, analysis, or interpretation of data; the writing of the manuscript; or the decision to publish the results.

References

1. Morrison, W.B. Microalloy steels—The beginning. *Mater. Sci. Technol.* **2009**, *25*, 1066–1073. [CrossRef]
2. Valdes, E.; Sellars, C.M. Influence of roughing rolling passes on kinetics of strain induced precipitation of Nb(C,N). *Mater. Sci. Technol.* **1991**, *7*, 622–630. [CrossRef]
3. Fujiyama, N.; Nishibata, T.; Seki, A.; Hirata, H.; Kojima, K.; Ogawa, K. Austenite grain growth simulation considering the solute-drag effect and pinning effect. *Sci. Technol. Adv. Mater.* **2017**, *18*, 88–95. [CrossRef] [PubMed]
4. DeArdo, A.J. Niobium in modern steels. *Int. Mater. Rev.* **2003**, *48*, 371–402. [CrossRef]
5. Gladman, T. *The Physical Metallurgy of Microalloyed Steels*, 1st ed.; Institute of Materials: London, UK, 1997; ISBN 0-910716-81-2.
6. Andersson, J.-O.; Helander, T.; Höglund, L.; Shi, P.; Sundman, B. Thermo-Calc & DICTRA, computational tools for materials science. *Calphad* **2002**, *26*, 273–312. [CrossRef]
7. Akhtar, M.; Khan, M.; Khan, S.; Afzal, A.; Subbiah, R.; Ahmad, S.; Husain, M.; Butt, M.; Othman, A.; Bakar, E. Determination of Non-Recrystallization Temperature for Niobium Microalloyed Steel. *Materials* **2021**, *14*, 2639. [CrossRef]
8. Zeng, R.; Huang, L.; Li, J.; Li, H.; Zhu, H.; Zhang, X. Quantification of multiple softening processes occurring during multi-stage thermoforming of high-strength steel. *Int. J. Plast.* **2019**, *120*, 64–87. [CrossRef]
9. Cho, S.-H.; Kang, K.-B.; Jonas, J.J. The Dynamic, Static and Metadynamic Recrystallization of a Nb-microalloyed Steel. *ISIJ Int.* **2001**, *41*, 63–69. [CrossRef]
10. Dos Santos, A.A.; Barbosa, J.V. Calculation of rolling force in the hot strip finishing mill using an empirical model. *Tecnol. Metal. Mater. Min.* **2020**, *17*, 149–156. [CrossRef]
11. Fernandez, A.I.; Uranga, P.; Lopez, B.; Rodrigues-Ibabe, J.M. Dynamic recrystallization behavior covering a wide austenite grain size range in Nb and Nb–Ti microalloyed steels. *Mater. Sci. Eng. A* **2003**, *361*, 367–376. [CrossRef]
12. Siwecki, T. Modelling of Microstructure Evolution during Recrystallization Controlled Rolling. *ISIJ Int.* **1992**, *32*, 368–376. [CrossRef]
13. Dutta, B.; Sellars, C.M. Effect of composition and process variables on Nb(C,N) precipitation in niobium microalloyed austenite. *Mater. Sci. Technol.* **1987**, *3*, 197–206. [CrossRef]
14. Dutta, B.; Valdes, E.; Sellars, C. Mechanism and kinetics of strain induced precipitation of Nb(C,N) in austenite. *Acta Met. Mater.* **1992**, *40*, 653–662. [CrossRef]
15. Guo, Z.L.; Miodownik, A. Modelling Deformation-Induced Precipitation Kinetics in Microalloyed Steels during Hot Rolling. *Mater. Sci. Forum* **2012**, *706–709*, 2728–2733. [CrossRef]
16. Liu, W.J. A new theory and kinetic modeling of strain-induced precipitation of Nb(CN) in microalloyed austenite. *Met. Mater. Trans. A* **1995**, *26*, 1641–1657. [CrossRef]
17. Dutta, B.; Sellars, C. Strengthening of austenite by niobium during hot rolling of Microalloyed steel. *Mater. Sci. Technol.* **1986**, *2*, 146–153. [CrossRef]
18. Foder, J.; Klančnik, G.; Burja, J.; Kokalj, S.; Bradaškja, B. Mean-Flow-Stress Analysis of Laboratory hot-rolled S1100QL Steel with minor Nb addition. *Mater. Technol.* **2020**, *54*, 901–908.
19. Sims, R.B. The Calculation of Roll Force and Torque in Hot Rolling Mills. *Proc. Inst. Mech. Eng.* **1954**, *168*, 191–200. [CrossRef]
20. Dimatteo, A.; Vannucci, M.; Colla, V. Prediction of Mean Flow Stress during Hot Strip Rolling Using Genetic Algorithms. *ISIJ Int.* **2014**, *54*, 171–178. [CrossRef]
21. Stalheim, D.G. Recrystallization behaviors in the production of structural steels. In Proceedings of the 52nd Rolling Seminar, ABM Week, Rio de Janeiro, Brazil, 17–21 August 2015; pp. 168–177. [CrossRef]

22. Stalheim, D.G.; Glodowski, R. Fundamentals of the Generation of Fine Grain As-rolled structural Steels. In Proceedings of the AIST International Symposium on the Recent Developments in Plate Steels, Winter Park, CO, USA, 19–22 June 2011; pp. 123–130.
23. Stalheim, D.G.; Barbosa, R.A.N.M.; Bastos, F.M.M.D.M.; Gorni, A.A.; Rebellato, M.A. Basic metallurgy/processing design concepts for optimized hot strip structural steel in yield strength from 300-700 MPa. In Proceedings of the 53rd Rolling Seminar, ABM Week, Rio de Janeiro, Brazil, 27–29 September 2016; pp. 31–41. [CrossRef]
24. Ding, W.; Jiang, Z.; Li, J.; Li, S.; Zha, C.; Bai, X.; Li, Q.; Zhang, G.; Stalheim, D. Research and development into low temperature toughness of large diameter heavy wall X80 pipeline steel at Shougang steel. In Proceedings of the IPC 2021, 9th International Pieline Conference, Calgary, AB, Canada, 24–28 September 2021; pp. 285–291. [CrossRef]
25. Bradaškja, B. Modelling of Strain Induced Precipitation in Micro Alloyed Steels during Continuous Casting. Ph.D. Thesis, University of Ljubljana, Ljubljana, Slovenia, 2011.
26. *EN ISO 6892-1*; Metallic Materials—Tensile Testing—Part 1: Method of Test at Room Temperature. European Committee for Standardization: Brussels, Belgium, 2019.
27. *EN ISO 148-1*; Metallic Materials—Charpy Pendulum Impact Test—Part 1: Test Method. European Committee for Standardization: Brussels, Belgium, 2016.
28. *EN 10025-2*; Hot Rolled Products of Structural Steels—Part 2: Technical Delivery Conditions for Non-Alloy Structural Steels. European Committee for Standardization: Brussels, Belgium, 2019.
29. Scales, M.; Anderson, J.; Kornuta, J.A.; Switzner, N.; Gonzalez, R.; Veloo, P. Accurate Estimation of Yield Strength and Ultimate Tensile Strength through Instrumented Indentation Testing and Chemical Composition Testing. *Materials* **2022**, *15*, 832. [CrossRef]
30. Back, J.G.; Engberg, G. Investigation of Parent Austenite Grains from Martensite Structure Using EBSD in a Wear Resistant Steel. *Materials* **2017**, *10*, 453. [CrossRef]
31. Reichert, J.M.; Militzer, M.; Poole, W.J.; Collins, L. A New A new approach using EBSD to quantitatively distinguish complex transformation products along the HAZ in X80 Linepipe steel. In Proceedings of the 10th International Pipeline Conference, Calgary, AB, Canada, 29 September–3 October 2014; Volume 3. [CrossRef]
32. Samuels, L.E. *Light Microscopy of Carbon Steels*, 2nd ed.; ASM International: Materials Park, OH, USA, 1999; ISBN 0-87170-655-5.
33. Rodriguez-Ibabe, J.M.; Wang, H.; Stahlheim, D.G.; Barbosa, R.A.N.M. Strategy for cost-effective alloy design optimization for strength and ductility properties of structural steels. *Tecnol. Metal. Mater. Min.* **2020**, *17*, 170–177. [CrossRef]
34. Annan, K.; Siyasiya, C.; Stumpf, W. The influence of niobium content on austenite grain growth in microalloyed steels. *J. S. Afr. Inst. Min. Met.* **2015**, *115*, 973–980. [CrossRef]
35. Buken, H.; Kozeschnik, E. A Model for Static Recrystallization with Simultaneous Precipitation and Solute Drag. *Met. Mater. Trans. A* **2016**, *48*, 2812–2818. [CrossRef]
36. Irvin, K.J.; Pickering, F.B.; Gladman, T. Grain-refined C-Mn Steels. *J. Iron Steel I* **1967**, 161–182.
37. Barbosa, R.; Boratto, F.; Yue, S.; Jonas, J.J. The influence of chemical composition on the recrystallisation behaviour of microalloyed steels. In Proceedings of the International Symposium on Processing, Microstructure and Properties of HSLA Steels, Pittsburgh, PA, USA, 3–5 November 1987; pp. 51–61.
38. Adamczyk, J.; Ozgowicz, W.; Wusatowski, R.; Kalinowska-Ozgowicz, E.; Grzyb, R. Boron-treated microalloyed quenched and tempered plates, their structure and properties. *J. Mater. Process. Technol.* **1997**, *64*, 1–8. [CrossRef]
39. Klančnik, G.; Foder, J.; Jan, P.; Klančnik, U. DTA study and thermodynamic prediction of the solidification interval of boron 500HB abrasion-resistant steel. *J. Therm. Anal.* **2021**, *147*, 1999–2011. [CrossRef]
40. Bernetič, J.; Bradaškja, B.; Kosec, G.; Kosec, B.; Bricelj, E. Centreline formation of the Nb(C,N) eutectic in 0.15% C; 0.0071% N; 0.022% Nb; 0.033% Al and 0.003% S Structural Steel. *Mater. Technol.* **2008**, *42*, 291–294.
41. *EN 10164:2004*; Steel Products with Improved Deformation Properties Perpendicular to the Surface of the Product—Technical Delivery Conditions. European Committee for Standardization: Brussels, Belgium, 2004.
42. Guo, B.; Fan, L.; Wang, Q.; Fu, Z.; Wang, Q.; Zhang, F. Effect of Finish Rolling Temperature on the Microstructure and Tensile Properties of Nb–Ti Microalloyed X90 Pipeline Steel. *Metals* **2016**, *6*, 323. [CrossRef]
43. Sandström, R.; Lagneborg, R. A model for hot working occurring by recrystallization. *Acta Met.* **1975**, *23*, 387–398. [CrossRef]
44. Baker, T.N. Titanium microalloyed steels. *Ironmak. Steelmak.* **2017**, *46*, 1–55. [CrossRef]
45. Militzer, M. 1.10—Thermomechanical Processed Steels. In *Comprehensive Materials Processing*; Material Science and Materials Engineering; Hashmi, S., Batalha, G.F., Van Tyne, C.J., Yilbas, B., Eds.; Elsevier: Amsterdam, The Netherlands, 2014; Volume 1. [CrossRef]